ISSN: 2454-9940

INTERNATIONAL JOURNAL OF APPLIED SCIENCE ENGINEERING AND MANAGEMENT

E-Mail :
editor.ijasem@gmail.com
editor@ijasem.org

www.ijasem.org

INTERNATIONAL JOURNAL OF APPLIED SCIENCE ENGINEERING AND MANAGEMENT

ISSN 2454-9940

www.ijasem.org

Vol 18, Issue 3, 2024

https://zenodo.org/records/14506032

An Architecture Derived from Biological Vision for Enhanced Low-Light Image Clarity

Dr.Valiki Vijaya Bhasker[1], Professor[1], Department of ECE, Siddhartha Institute of Technology & Sciences, Telangana, India

Dr.Pulime Satyanarayana[2], Professor[2], Department of CSE, Siddhartha Institute of Technology & Sciences, Telangana, India.

Abstract—

When it comes to situations with low sight, image improvement is a crucial pre-processing stage for many computer vision apps. In this paper, we elaborate on low dynamic range (LDR) image improvement and high dynamic range (HDR) image tone mapping are two applications of a united two-pathway paradigm that draws inspiration from biological vision, particularly the early visual processes. There are two distinct visual paths that receive the incoming picture. These are the structure-pathway and the detail-pathway, which are analogous to the M-pathway and the P-pathway in the early visual system. To manage visually complex landscapes with changing lighting conditions, the structure-pathway employs an expanded biological normalization model to combine global and local brightness adaptation. However, in the detail-pathway, based on local energy loading, the increase of details and the reduction of local cacophony are accomplished. Finally, the results of the structure-pathway and the detail-pathway are combined to improve the picture in dim light. In addition, with some tweaks, the suggested model can be used for tone mapping of HDR pictures. Extensive tests on three datasets (two LDR picture datasets and one HDR scene dataset) demonstrate that the suggested model is capable of effectively completing the aforementioned visual improvement tasks, while also outperforming the associated state-of-the-art techniques.

I. INTRODUCTION

In many computer vision uses, improving images is a crucial first stage in the processing pipeline. In particular, twilight or low-light photographs typically experience the low vision and lack of contrast. The effective handling of visual disruptions in complicated visual situations by the human visual system (HVS) is an intriguing problem. Early visual processing, which includes visual adaptation processes, is generally acknowledged to be crucial in the area of visual neurobiology [1]. From a technical perspective, the fast development of machine learning technologies (such as deep learning) has also allowed academics to make significant strides in a variety of computer vision-related uses [2]. When Analyzing low-light or nocturnal images, however, even the best-trained models can struggle due to the presence of noise and other distracting factors. High reliability of scene analysis techniques when confronted with low-light or nocturnal situations depends on effective picture improvement [3].

Most traditional approaches to picture improvement center on tweaking the distribution of raw photos in order to bring out more latent features. Histogram equalization (HE) and variants of it (such as adaptive histogram equalization (AHE) [4, bi-histogram equalization (BHE) [5, and contrast limited adaptive histogram equalization (CLAHE) [6]) attempt to modify the histogram's distribution by enforcing various regularization terms. Nonlinear data mapping for visual improvement is also performed by contextual and variation contrast enhancement techniques [7]. In the role of a symbol One, in [8], the stacked difference depiction of a 2D histogram is used to suggest a contrast improvement technique. However, the well-known Retime theory postulates that a visual picture can be broken down into two components—reflectance and illumination—because it was influenced by the molecular processes involved in the early visual system [9]. Based on the Retime theory, Rahman et al. have created several variants for picture improvement, such as single-scale Retinex (SSR) [10], multi-scale Retinex (MSR) [11], etc. To maintain the natural look of pictures captured with non-uniform lighting, Wang et al. [12] suggested a technique that involves plotting the illumination with a bi-log transformation to strike a compromise between detail and naturalness. Recent work [13] has demonstrated that a weighted variation model for simultaneous reflectance and light estimation (SRIE) can better maintain features while dampening sounds. Both Park et al. [14] and Li et al. [15] suggested methods for improving low-light

INTERNATIONAL JOURNAL OF APPLIED SCIENCE ENGINEERING AND MANAGEMENT

ISSN 2454-9940

www.ijasem.org

Vol 18, Issue 3, 2024

https://zenodo.org/records/14506032

images using Retime models that rely on variation optimization and take noise maps into account. In a similar vein, Guo et al.'s suggested technique [16] for enhancing low-light images with a well-constructed lighting map achieves good performance and economy. In order to process information quickly and effectively, the organic vision system has developed into a highly effective system. Enhance the visible data that is being fed into the system. The divided normalization, as a standard brain calculation, has been proposed to play an important role in visual adaptation [37] by a number of studies. The retina's primary role is to pre-process the visual stimuli [1, 38]; it is also regarded the first stage in visual information processing in the human visual system. It has been hypothesized that a number of significant cellular processes work to increase the legibility of visible data.

Visual adjustment using a norm-diverging approach. The retina's local adaptation mechanisms allow it to adjust to the wide variety of visual image intensities within the capabilities of the brain's computational apparatus [1]. Furthermore, the mean luminance and contrast on natural images are regarded to be crucial factors for fast adaptation in the eye [1, 39]. More and more research over the past few years suggests that divided normalization may be a standard brain calculation that contributes to a variety of functions, including visual light adaptation [37, 40]. Divisive normalization models have been shown to contribute to picture improvement tasks in a number of publications [41, 42]. In the primary sensory system, there are two distinct routes. Further vision processing relies heavily on the retina's parallel information processing pathways [43]. Just to recap, the Midget cells and Parasol cells [[43], [44]] in the retina analyze incoming vision information. Midget cells, in particular, are specialized for encoding high-frequency information, such as the finer features and background sounds of visual images, due to their tiny receptive fields (RFs). However, Parasol cells excel at encoding low-frequency information (i.e., the world patterns of pictures) due to their higher RFs [44]. There are two major neural pathways in the developing visual system, the magnocellular pathway (M-pathway) and the parvocellular pathway (P-pathway). Many fields of neurobiology and quantitative modeling have demonstrated the benefits of the two-pathway approach and visual adaptation. For tone mapping, for instance, Meylan et al. [45] have suggested a model of ocular local adaptation that can be applied immediately to the sensor mosaic pictures. LDR picture improvement and/or HDR tone mapping visual adaptation models [42, 46, and 47] have been created recently. However, picture segmentation as a technique has

As shown in Figure 1, this study takes into account a variety of eye improvement activities.

Commonplace applications include noise reduction (demising images) [48] and JPEG distortion removal [50]. In this article, we examine how to improve images in two distinct ways: (1) with low-dynamic-range improvement and (2) with high-dynamic-range tone mapping. The end result of these two activities should be an increase in picture clarity and intricacy. Input pictures for LDR image improvement typically have low dynamic ranges, such as a ratio of 256:1 or less. In comparison, HDR tone mapping typically requires raw pictures with much larger dynamic ranges (1000:1 or more). Therefore, dynamic range reduction is an integral part of HDR tone mapping in order to accommodate the lower dynamic range of display devices. In Fig. 1, the outcomes of the technique suggested in this article are displayed alongside three instances of the aforementioned improvement tasks. We aimed to develop a biologically influenced, rather than a biologically based, approach to the image processing tasks at hand. The suggested approach is motivated by only a subset of the visual information processing processes. We also adapted other biological characteristics for further processing, in addition to the property that prompted the geographic scale segmentation of pictures into low- and high-frequency channels. As an illustration, the low-frequency channel's global and local brightness adaptation was combined through the introduction of an expanded normalization model. In conclusion, the following are the main accomplishments of this paper: (1) we constructed a uniform structure for LDR image

INTERNATIONAL JOURNAL OF APPLIED SCIENCE ENGINEERING AND MANAGEMENT

ISSN 2454-9940

www.ijasem.org

Vol 18, Issue 3, 2024

https://zenodo.org/records/14506032

enhancement, HDR tone mapping, and other image enhancement jobs. Mapping. The processes of the early visual pathway provided inspiration for the parallel paths approach, which can be readily applied with the help of general structure-texture deconstruction techniques. (2) Motivated by the latest physiological results, we suggested an expansion of the Naka-Rushton equation [40] that incorporates the local and global adaptation factors, resulting in greater adaptability and enhanced performance during ocular local adaptation. Thirdly, this article proposes a novel approach to estimating noise from a global to local perspective. We determine the noise level in two stages (from global to local), which leads to improved performance in terms of both noise reduction and information retention.

II. IMAGE ENHANCEMENT FRAMEWORK

In this study, we suggested a picture improvement paradigm based on the parallel paths present in the developing visual system.

Figure 2: The conceptual outline of the suggested model, which was developed with reference to organic vision processes.

Structure-pathway and detail-pathway are two examples of how we process sensory information. This is a brief outline of the suggested strategy. Fig. 2. The initial step is to split the incoming sensory data into these two independent channels. In particular, the structure pathway transmits and processes low-frequency information (such as luminance), and then uses visual adaptation mechanisms to bring the image's brightness up to a usable level. In addition, the high-frequency information is transferred along a detail-pathway where noise is reduced and the underlying structure is maintained. (e.g., the details and noises). The merged results of the structure-pathway and detail-pathway are then used to improve brightness, reduce noise, and highlight finer details.

A. Pathway Separation with Global Noise Estimation

Images captured in low light, particularly at night, are notoriously noisy. The sounds in such pictures need to be reduced or eliminated during the processing stage so that the final product is more pleasing to the eye. The editing of improving images. The difficulty of noise reduction or removal is typically increased when scene lighting is improved immediately. By dividing the visual processing into distinct channels, adjustments to the structure-pathway's brightness and the detail-pathway's noise reduction can be made independently. Biologically speaking, Li et al. [51] discovered that the response of some LGN cells in cats to the stimulus of dispersedly distributed dots is relatively feeble compared to the response to the stimulus of compactly distributed dots (e.g., the dispersedly distributed dots are compressed into a line). This physiological observation hints at the possibility of utilizing some LGN cells (typically for high-frequency information processing) for noise suppression while maintaining detail. From a technical standpoint, demising can be accomplished using picture decomposition techniques. In order to remove the noise layer, TV-based picture segmentation is used in the noise reduction method suggested by Rudin et al. [49].

While other works simply discard the deconstructed detail layer, we instead use noise suppression and detail restoration techniques. To do this, we use a total-variation (TV) energy based image segmentation technique [48] to split the original picture in two. Firstly, superimposing these two levels yields the input picture IC(x; y). Base

$I^c_{base}(x,y)$ and detail layers $I^c_{detail}(x,y)$, i.e.,

$$I^c(x,y) = I^c_{base}(x,y) + I^c_{detail}(x,y) \quad (1)$$

The basic layer is then achieved by minimizing the following objective function, which is based on the TV regularization suggested in [49].

INTERNATIONAL JOURNAL OF APPLIED SCIENCE ENGINEERING AND MANAGEMENT

ISSN 2454-9940

www.ijasem.org

Vol 18, Issue 3, 2024

https://zenodo.org/records/14506032

$$\min_{I^c_{base}} \sum_{(x,y)} \left(I^c_{base}(x,y) - I^c(x,y)\right)^2 + \lambda^c \left|\nabla I^c_{base}(x,y)\right| \quad (2)$$

This objective function has two terms: the first is a difference term tailored to the texture component that is meant to maintain the semantic structure, and the second is a term that is meant to maximize some other criterion. One is a total-variation-based regularization word that sets a bound on the level of information in the picture [49] Since the low-frequency data won't interfere, noise reduction and detail enhancement can be carried out in the detail-pathway It is possible to calculate the worldwide noise measurement ("c") using [52].

$$\varepsilon^c = \sqrt{\frac{\pi}{2}} \frac{1}{6(W-2)(H-2)} \sum_{(x,y)} \left|\left(I^c * N_s\right)(x,y)\right| \quad (3)$$

$$N_s = \begin{bmatrix} 1 & -2 & 1 \\ -2 & 4 & -2 \\ 1 & -2 & 1 \end{bmatrix} \quad (4)$$

C 2 = Fr; g; BG, where _ is the convolution function. The image's breadth (in pixels) and height (in pixels) are denoted by W and H, correspondingly. (IC). we have a general idea of the with (4). High-frequency component's amplitude, a metric for setting the regularization parameter (2). Therefore, the high-frequency component to be routed down the detail-pathway can be determined in a flexible fashion by using the suggested technique.

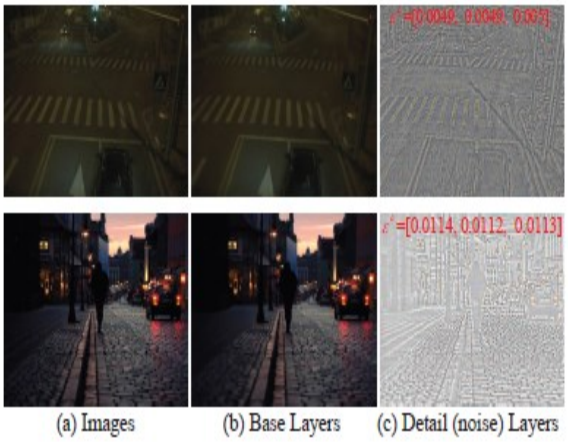

(a) Images (b) Base Layers (c) Detail (noise) Layers

Decomposition examples with global noise prediction are shown in Figure 3. The worldwide noise estimates for the R, G, and B channels can be seen in the accompanying detail images. By working out (2), we can acquire the scene's foundational layer, which contains the bulk of the scene's structure. The stratum of finer information can then be easily extracted by

$$I^c_{detail}(x,y) = I^c(x,y) - I^c_{base}(x,y) \quad (5)$$

The global noise estimation and picture segmentation samples are displayed in Fig. 3. Figure 3 elucidates the primary partitioning of brightness data into the foundational stratum, with the latter housing the finer points and any accompanying sounds. Adjusting the lighting in the structure-pathway won't increase the sounds already present in the detail-pathway because the base-layer's information will have been moved there. On the other hand, as will become clear below, noise reduction in the detail-pathway will be aided by the separation of the detail layer from the brightness layer. It's important to realize that, from the perspective of image processing, even in the image improvement areas, dividing a picture into different sizes is a universal technique [53]. For instance, the image analysis field has made extensive use of structure-texture decomposition [48]. In contrast, we reexamined structure-texture decomposition from the perspective of the organic vision system in this study. We also used global noise estimation for parameter setup to accomplish flexible segmentation of images across varying noise conditions.

B. Luminance Adaptation in structure-pathway

Our model's structure-pathway accomplishes eye adaptation and light regulation. The provided image's brightness data is extracted by inverting the image's base layer. From RGB color space to HSV color space, where the V channel is retrieved as the brightness data. The method (Hex cone Model) described in [54] is used to convert the RGB raw picture to the HSV color space using the MATLAB image tools. Using this technique, you can get values for H, S, and V that are all equal and fall within [0,1]. This color change is commonly used for picture improvement jobs because it yields good outcomes with minimal quality loss [13, 15].

$$R(x,y) = \frac{L(x,y)^n}{L(x,y)^n + \sigma^n} \quad (6)$$

Where the visual input strength L(x; y). The average of the S-shaped curve on the log input is determined by the global adaptation factor _ (a constant showing the input light intensity). Brightness scale (lower side

INTERNATIONAL JOURNAL OF APPLIED SCIENCE ENGINEERING AND MANAGEMENT

ISSN 2454-9940

www.ijasem.org

Vol 18, Issue 3, 2024

https://zenodo.org/records/14506032

of Fig. The worldwide contrast can be scaled up or down depending on the value of n, as shown in Fig.4 (right). Therefore, adjusting _ and n to match the visual images or areas used as input can be thought of as the visual adaptation processing. A straightforward and effective method for eye adaptation is provided by the standard NR equation in (6). However, when it comes to adjusting to nearby sensory cues, this NR equation is notoriously ineffective. In the case of nocturnal images in particular, a worldwide adaptation level (_) is insufficient for accurately capturing the regional details of the widely changing lighting conditions. The neural reactions in the fly smell system have recently been described with a novel equation that includes a local component [55]. It's important to remember that human and insect perception is very different. Although there is great variation in vision systems across animals, some research suggests that normalization may be a fundamental brain calculation [37]. This motivates us to modify the traditional NR equation in this research, fusing the local and global visual adaptations in a weighted way.

Since the traditional Naka-Rushton is a global equation [45], we updated the NR equation computationally by incorporating the geographic interdependence in the light control.

$$L_{out}(x,y) = \frac{L_{in}(x,y)^n}{L_{in}(x,y)^n + \omega_l(x,y)\cdot\sigma_l(x,y)^n + \omega_g(x,y)\cdot\sigma_g{}^n} \quad (7)$$

In (7), Lin(x; y) represents the image's luminance channel in the underlying layer. The degree of eye response depends on two factors: In this context, _l(x; y) refers to the local adaptation level, which , and _g is an approximated global adaptation level based on the entire picture, both of which change depending on their respective local image areas. Therefore, our approach begins by estimating the global and local adaptation factors for an initial picture. The global adaptation factor (!g(x; y)) and the local adaptation factor (!l(x; y)) are weighted according to the local brightness of the image. The modified brightness map (Lout(x; y)) is obtained by computing the global and local adaptation factors, as well as the weights. First, we'll use M_ for the average luminosity across all pixels in the image's brightness channel and S_ for the standard deviation. The formula for determining the worldwide adaptation factor, _g, is

$$\sigma_g = \frac{M_g}{1+w_s \cdot S_g} \quad (8)$$

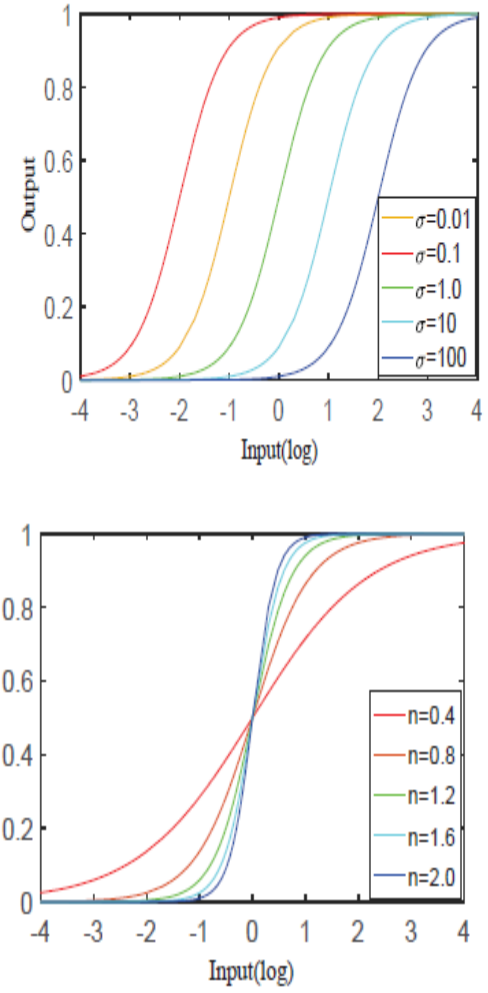

Figure 4: Naka-Rushton equation-generated response patterns in (6). The sensitive curves for changing _ while keeping n constant, on the left, and the sensitive curves for changing n while keeping _ constant, on the right.

Where! S is a measure that determines how much of an effect the variation as measured by the standard deviation. We merely removed the cells with values outside of the range of 0.5% _ 99.5% luminosity level to remove the outliers from the mean and standard deviation calculations. The brightness map's global mean (Mg) and standard deviation (Sg) are used to calculate the global adaptation factor (_g), which is defined as (8). As a consequence, a lower _g

INTERNATIONAL JOURNAL OF APPLIED SCIENCE ENGINEERING AND MANAGEMENT

ISSN 2454-9940

www.ijasem.org

Vol 18, Issue 3, 2024

https://zenodo.org/records/14506032

creates a greater brightness increase in a darkened environment, and vice versa. For pictures with a bimodal histogram distribution—scenes in which there are both dark and light areas—the standard deviation term (Sg) is used to adjust the global adaptation factor calculation. Overestimating the global adaptation factor would be wasteful for the dark areas if only the global mean were used, and a picture with more light pixels would result in a bigger global mean. However, since Sg is typically less than 1.0, its impact on most scenarios is minimal. Furthermore, by settings = 0, the standard deviation (Sg) word can be conveniently removed from some contexts.

$$\sigma_l(x,y) = \sigma_g \cdot \frac{L_{in}(x,y)}{1+w_s \cdot S_l(x,y)} \tag{9}$$

$$\omega_g(x,y) = L_{in}(x,y)^k \tag{10}$$

$$\omega_l(x,y) = 1 - \omega_g(x,y) \tag{11}$$

One can adjust the weight of the global and local adaptation terms by adjusting the number k. In the part titled "Experiments," we'll look at how changing k affects the end findings. In (7), the inclination of the S-shaped arcs is determined by the value of n, which also affects the improvement in contrast. The global adaptation word (_g) is used in this study to calculate the global contrast enhancement factor, which is expressed as

$$n = \exp(\sigma_g) \tag{12}$$

Where n will fall roughly between [1, 2.7] because _g's domain is [0, 1]. As can be seen in Fig. 4 for the arcs of various intensities, this range is acceptable for global contrast scaling. Since the approximated global adaptation term (_g) is a measure of the overall brightness of the input scene, it follows as an implied restriction that black scenes should not have their global contrast increased to excessive levels, lest the details in those areas be lost Furthermore, dynamic range modification may lessen the local difference in specific areas. Therefore, in order to bring out the finer features in the picture, we construct an extra and discretionary local contrast enhancement algorithm using a difference of Gaussian (DoG) filter, which is represented as

$$L'_{out}(x,y) = (1+\omega_{dog}) \cdot L_{out}(x,y) - \omega_{dog} \cdot (L_{out} * G)(x,y) \tag{13}$$

$$G(x,y) = \frac{1}{2\pi\delta_c^{\,2}} \exp\left(-\frac{x^2+y^2}{2\delta_c^{\,2}}\right) \tag{14}$$

Where G(x; y) represents a Gaussian filter and _ stands for the convolution function. The study's standard variation was determined by

Figure 5 shows some instances of structure-pathway illumination tweaking. In which _c = 21 for black-and-white night shots and _c = 51 for high dynamic range pictures. In In addition, throughout this paper's trials, we maintained the constant value of! Dog = 0:5. The improved brightness maps are then normalized after the standard post-processing step of removing the pixels outside the [0, 1] range. The end outcome was achieved by converting the improved luminance map (L0 out(x; y)) from the HSV color space to the RGB color space. However, we notice that for some pictures with very intense light sources, getting the output RGB image transformed from HSV (HSV! RGB) may result in an over-saturated look. (See Fig. 13). Thus, we propose an alternative, effective technique for minimizing color shift when converting brightness values back into a color picture, by introducing an exponent s to regulate color saturation [17]. This procedure yields the finished transformed color picture Co base(x; y).

$$O^c_{base}(x,y) = L'_{out}(x,y)\left(\frac{I^c_{base}(x,y)}{L_{in}(x,y)}\right)^s \tag{15}$$

INTERNATIONAL JOURNAL OF APPLIED SCIENCE ENGINEERING AND MANAGEMENT

ISSN 2454-9940

www.ijasem.org

Vol 18, Issue 3, 2024

https://zenodo.org/records/14506032

C. Noise reduction in the detail-pathway while preserving detail.

In low-light pictures, noise contamination is particularly pronounced and often cannot be eliminated. Cams of a poor grade; a slang term. Noise reduction is an essential process for making the most of the improved nocturnal landscapes. When applied to high-resolution daytime pictures, a number of demising techniques (such as Non-local Mean [56] and BM3D [57]) have shown promising results. Some improvement techniques use demising operators tailored to low-light pictures as post-processing to eliminate sounds [16]. Demising operations are able to eliminate sounds, but they can also distort features in low resolution pictures. (See Fig. 8). In this research, we employ a noise reduction approach rather than a noise removal strategy to reduce background noise while keeping finer features intact. Additionally, we employ noise reduction in the detail-pathway, which helps to dampen the impact of low-frequency data. High-frequency features and sounds are extracted via the structure-texture decomposition in (1)-(4). As a result, in we presume a globally consistent noise level in order to make accurate estimates of the local sounds. Then, the energy density in the detail layer can be used as a rough measure of the background noise. We assume that the regions with the lowest local energy reflect the image's noise level since these regions are typically flat (e.g., the sky) and contain most of the sounds. On the other hand, higher-energy areas should result from a synthesis of local particulars and sounds.

Therefore, we compare the local energy of the detail layer with the weights of detail retention (_c(x; y)).

$$\mu^c(x,y) = (|I^c_{detail}| * G)(x,y) \qquad (16)$$

$$O^c_{detail}(x,y) = I^c_{detail}(x,y) \cdot \mu^c(x,y) \qquad (17)$$

Noise reduction in the detail-pathway is illustrated in Fig. 6. Decomposing a twilight picture reveals that its detail layer typically includes high levels of noise, even in relatively uniform areas like the heavens (Fig. 6(b)). As can be seen in Fig. 6, local energy, as stated in (16), provides a good approximation of the preservation weights. (c). Figure 6(d) depicts processed detail maps with noise suppression that preserves structure features, such as houses, while successfully suppressing noise in flat areas.

Final Image Reconstruction (D)

The brightness improved map from the structure-pathway and the detail-map with noise reduction from the detail-pathway is the results of processing the original picture. The finished product, including the treated basic layer and detail layer, can be obtained by

$$O^c(x,y) = O^c_{base}(x,y) + w_d \cdot O^c_{detail}(x,y) \qquad (18)$$

In which WD is used to strike a happy medium between boosting details and reducing cacophony. Following this, we will acquire the ultimate improved outcome map by trimming and adjusting the pixels. In the context of a dark or dim picture.

Figure 6: Noise reduction in the detail layer that preserves fine details. Keep in mind that in order to more clearly illustrate the impact of noise reduction, we only show the pixels with positive values in the detail image, despite the fact that the other pixels (with negative values) have the same effect. Details are retained while noise is reduced in (a) nocturnal pictures, (b) detail maps (only the positive pixels), (c) detail retention weights based on local noise estimation, and (d) detail maps.

E. Tone Mapping Refinement Expansion

The contrast ranges in the HDR images may be exceptionally broad. When applied to HDR images,

INTERNATIONAL JOURNAL OF APPLIED SCIENCE ENGINEERING AND MANAGEMENT

ISSN 2454-9940

www.ijasem.org

Vol 18, Issue 3, 2024

https://zenodo.org/records/14506032

we include the following additional stages in the above-described suggested method: Logarithmic normalization as a preprocess, removal of detail-pathway processing, and adaptive gamma correction as a post process. First, the original picture is converted to the HSV color space, and from there we immediately extract the luminance channel (Lin(x; y)). Logarithmic rescaling is used as a pre-processing phase to bring the high dynamic range down to [0, 1], and then the logarithmically normalized picture is passed on to the suggested framework [46] for further improvement, avoiding the uneven dynamic ranges of the raw images.

$$L_{\log}(x,y) = \log_{\alpha}(L_{in}(x,y)+1) \qquad (19)$$

Where _ = max (Lin(x, y)) + 1 is used to accommodate situations with varying dynamic ranges, resulting in a nonlinear compression of the brightness range of Llog to 0 _ 1.0. In HDR compression, we bypass both the picture segmentation and detail-pathway processing steps, which are typically used to reduce noise. The reason for this is that high dynamic range (HDR) images typically have higher clarity and less noise. The luminance map is compressed using the formulas (7)–(14), where Llog is the log normalized luminance channel.

The local dynamic range of the compressed luminance map is then corrected using an extra adaptive gamma adjustment applied to the compressed luminance channel in an effort to further enhance HDR compression. We make educated guesses about the adjusted gamma settings for various scenarios by

$$\gamma = \frac{median(L'_{out})}{mean(L'_{out})} \qquad (20)$$

$$L^{*}_{out}(x,y) = L'_{out}(x,y)^{\gamma} \qquad (21)$$

Finally, L_ out(x, y) could be reconstructed back into RGB color space with (15).

III. EXPERIMENTS

Here, we'll show how well the suggested technique works by applying it to two visual improvement-related tasks: (1) LDR picture enhancement, and (2) HDR scene tone mapping.

A. Tuning the Dials

The unconstrained parameters in our model are assigned experimentally to the values ws = 5:0 in (equations) (8) and (9), k = 0:2 in (equation) (10), and wd = 5:0 in (equation) (11). (18). First, since S_ is typically much less than 1.0, the impact of ws on most scenarios is minimal. In particular, the stability when confronted with images with various brightness distributions is enhanced by the contrast-aware determination of the adaptation factors in (8)-(9). In contrast, increasing ws can reduce the value of the global component and enhance the resulting scene's brightness in situations with a big S_. Figure 7 (first row) demonstrates that improved pictures with contrast-aware estimation of the adaptation factors (with ws = 5:0 or 10:0) are lighter than those without contrast-aware estimation (i.e. ws = 0). In the following tests, we use ws of 5:0 to see what happens to the system.

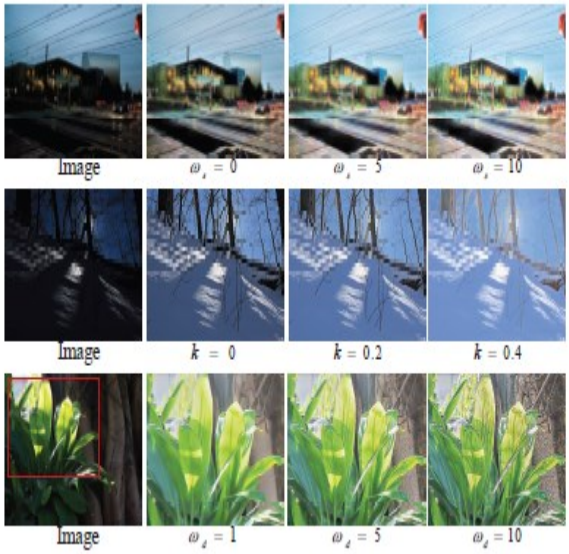

Figure 7: Outcomes as a function of the primary factors. First column: change ws while holding k = 0:2 and WD = 5:0 constant; in the second column, keep ws = 5:0 and WD = 5:0 while varying k; the fifth to last column: ws = 5, WD = 0. And k = 0:2.
Also, the value k in (10) determines how much dynamic range is compressed; a higher k results in a more drastic reduction in dynamic range. Figure 7 depicts the impact of k on the outcomes. (The second row). All subsequent tests will have k = 0:2 to prevent excessive compression of the dynamic range.

INTERNATIONAL JOURNAL OF APPLIED SCIENCE ENGINEERING AND MANAGEMENT

ISSN 2454-9940

www.ijasem.org

Vol 18, Issue 3, 2024

https://zenodo.org/records/14506032

In particular, when k = 0 (hence, g = 1:0 and! l = 0), the new NR equation (7) degenerates to the old one. (6). Thus, the benefits of our updated NR equation, which results in further lightening the black areas, can be seen in Fig. 7 (the second row). Last but not least, the LDR picture improvement jobs make use of the option WD, which determines how much information, is added. To prevent excessive amplification in the subsequent tests, we set WD = 5:0. (See Fig. 7, the last row).

B. Low-Dimensional Reflectance (LDR) Image Enhance

In this work, we conducted an evaluation of existing techniques for the LDR picture improvement assignment using two datasets (Knight and LDRpoor). Specifically, "Knight" refers to the 100 pictures [59] from the PKU-EAQA collection that was taken at night, the vast majority of which had a resolution of 400x300 pixels.

Visit https://www.pkuml.org/resources/pku-eaqa. Aspx to access this information. Other low dynamic range (LDR) pictures are labeled as "LDRpoor." including 73 photos taken by us in low-light circumstances. Several recently published studies, such as LIME [16], LDR [8], and Division Channel [60], used these pictures to assess their respective image improvement techniques. The writers' WebPages 123 were mined for all the pictures.

We substitute the noise eliminating with the noise reducing in the algorithmic flow of the detail-pathway, as previously described, in contrast to prior techniques that introduce an additional demising operator after the image enhancement (such as LIME [16]). An illustration of noise cancellation from this article is provided in Figure 8. If we look at Fig. 8(b), we can see that immediately increasing the brightness of nocturnal images also increases the noises, and if we look at Fig. 8(c), we can see that using an additional demising operator (BM3D [57]) can eliminate the noises, but it can also introduce new diseases or obscure important features. In comparison, the suggested approach can effectively strike a compromise between enhancing brightness, reducing noise, and maintaining fine detail (see Figure 8(d)). Close inspection of the middle row's zoomed-in regions reveals that the extra demising operator is unable to effectively eliminate some block sounds typically found in the low-resolution night images' darker areas. Conversely, the demising algorithm would over-smooth the structure features in the zoomed-in local areas in the bottom row. (e.g., the cloud in sky). The suggested technique, on the other hand, is able to not only reduce the block sounds in the shadowy areas, but to also maintain or even improve the relevant structure details.

C. HDR tone mapping

We concluded by testing the refined version of the suggested technique on the tone-mapping assignment. High-dynamic-range (HDR) pictures feature a broad variety of tonalities.

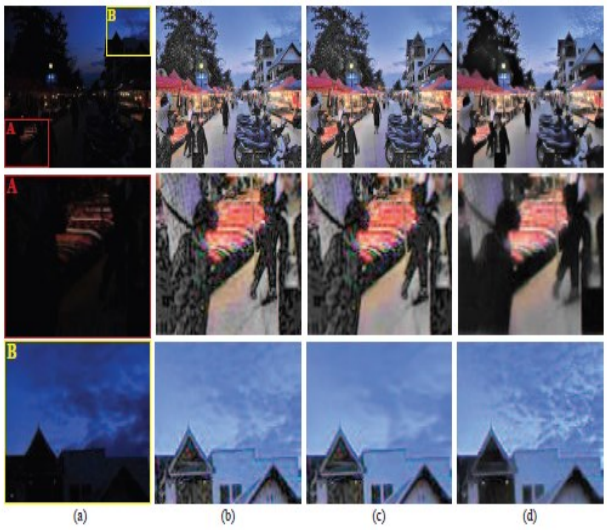

Figure 8 shows how our model stacks up against those that include a demising algorithm in order to reduce noise. pictures (a), (b), (c), and (d) show the impact of the suggested detail-preserved noise reduction on (a) and (b), respectively, as well as the original pictures (a) and (b).

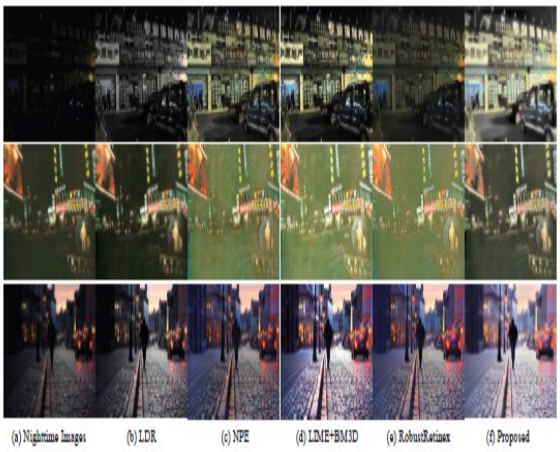

INTERNATIONAL JOURNAL OF APPLIED SCIENCE ENGINEERING AND MANAGEMENT

ISSN 2454-9940

www.ijasem.org

Vol 18, Issue 3, 2024

https://zenodo.org/records/14506032

Figure 9 shows how the suggested approach stacks up against some other popular options, such as LDR [8], NPE [12], LIME+BM3D [16], and RobustRetinex [15]. Causes LDR picture enhancement techniques to fail to work as intended. With the straightforward methods for with the fine-tuning outlined in Section II-E, our technique works well for HDR tone mapping. Meylan's adaptive Retime [18], a standard Retinexbased approach motivated by the organic vision system, is contrasted with our model's findings in Fig. 12. Moylan's technique successfully reduces the dynamic range while maintaining the image's brightness. Moylan's technique, on the other hand, typically causes a noticeable change in hue. The dynamic range reduction, contrast distortion, and color shift rectification are all well-balanced in our approach. And as you can see in Fig. 13, we also contrasted the results of post-processing (with and without color shift adjustment) and the use of various color schemes. When comparing the CIELAB and HSV color spaces, we see that while the former yields passable outcomes (Fig. 13(b)), the latter is less effective (Fig. 13(d)). Piecewise functions are used in the CIELAB color space calculation stages to acquire brightness information. As a result, the pictures utilized herein may exhibit an imbalance of brightness between very brilliant and very black areas. We also conducted tests on a few different species

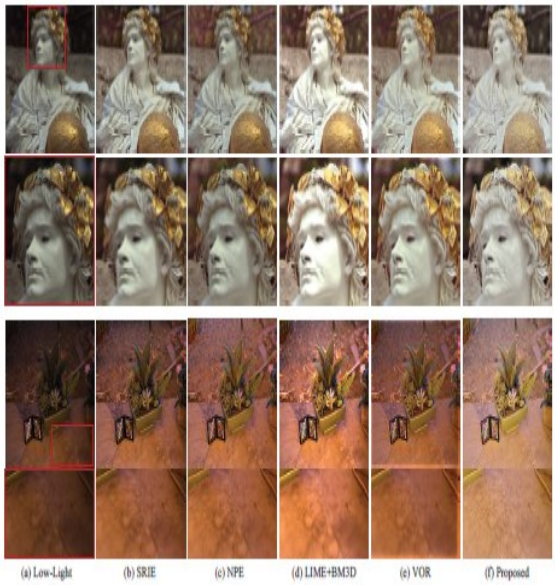

Figure 10 provides a graphical contrast between the findings obtained using the suggested approach and those obtained using SRIE [13], NEP [12], LIME+BM3D [16], and VOR [14].

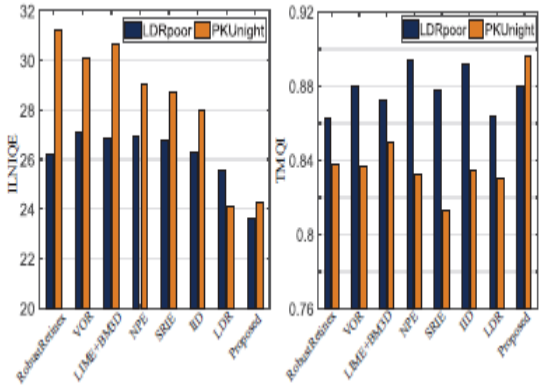

Figure 11 shows a quantitative evaluation of several LDR improvement techniques using the ILNIQE and TMQI measures. NPE [12], LDR [8], SRIE [13], VOR [14], and IID [58] are all contrasted here. Combining LIME and BM3D [16] and the RobustRetinex technique [15]. We have tried a number of different conceivable color spaces (such as the McLeod-Boynton [66] and DKL color space [67]) without success. Extracting brightness in a McLeod-Boynton or DKL color space is highly dependent on the L and M impulses (corresponding to the R and G channels of an RGB picture). In scenes with a lot of blue, this could significantly understate the B channel's input and lead to a lot of variation. Images with prominent light sources often look oversaturated when converted straight from HSV to RGB color space using the compressed luminance map (Fig. 13(c)). Figure 13(d) shows improved naturalness with the straightforward color shift adjustment outlined in (15). For these reasons, and because it is simple to comprehend and compute, we use the HSV color space for brightness extraction.

Tone mapping efficacy was also assessed on the HDR Photographic Survey (HDRPS) [68] dataset, which consists of 105 HDR photos and can be obtained from the website http: //rit-mcsl.org/fairchild/HDR.html. Figure 14 provides an additional set of observations with additional prototypical HDR tone mapping approaches. As we can see, the suggested technique achieves a nice middle ground between enhancing details and keeping things looking natural. In order to objectively assess the efficacy of tone mapping, we used a commonly used objective measure (i.e., the Tone Mapped Image Quality Index, TMQI [62]) in

INTERNATIONAL JOURNAL OF APPLIED SCIENCE ENGINEERING AND MANAGEMENT

ISSN 2454-9940

www.ijasem.org

Vol 18, Issue 3, 2024

https://zenodo.org/records/14506032

addition to the subjective evaluation. There is a strong relationship between the TMQI's combined structural integrity (integrity) and naturalness assessment (NSS) and the subjective rating scores [62]. The average TMQI, Fidelity, and NSS ratings for all 105 HDR pictures in the HDRPS collection are shown in Table I below. We see that our approach gets results that are comparable to those obtained by Durand et al. [20] and Liang et al. [65], but marginally inferior to those obtained by Shibata et al. [64]. Figure 14 shows that Durand et al.'s [20] technique typically produces over-saturated outcomes, which diminishes the naturalness of pictures. While Shibata et al.'s [64] approach yields excellent TMQI, Fidelity, and NSS ratings, its output (shown in Fig. 14) appears over-enhanced at the margins and is plagued by severe halo distortions. Accordingly, when the subjective rating is combined with the objective measure, the suggested approach achieves results that are competitive with those of current state-of-the-art techniques such as those presented by Liang et al. [65].

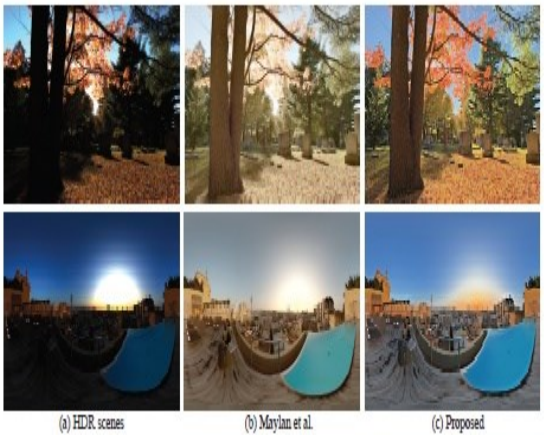

Moylan's modified Retime [18] is shown for comparison in Fig. 12. To better display the details in the landscapes, the HDR pictures used as input are linearly resized.

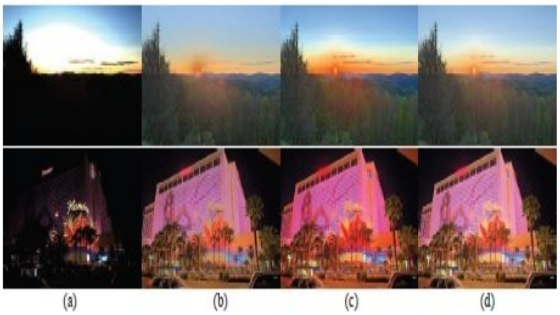

Figure 13: After-effects of using various color schemes. (a) HDR scenes as input, (b) luminance extracted in CIELAB color space and post-processed with color shift correction, (c) luminance extracted in HSV color space and output images obtained in HSV!RGB (i.e. post-processing without color shift correction), and (d) luminance extracted in HSV color space and post-processed with color shift correction. Input HDR pictures are resized, so keep that in mind. In a logical progression that makes the scene elements readily apparent.

Table I shows the results of a quantitative analysis of several tone mapping methods.

Methods	Durand	Kuang	Shan	Oskarsson	Shibata	Liang	ADRA	Proposed
TMQI	0.8588	0.7892	0.8261	0.8376	**0.8773**	0.8575	0.7735	0.8519
Fidelity	**0.8744**	0.818	0.8236	0.8067	0.8472	0.8013	0.7437	0.7890
NSS	0.3671	0.1536	0.2871	0.3654	**0.4946**	0.4808	0.1592	0.4543

4200 x 2800 is the pixel count. Table II shows that the suggested method is very computationally efficient, much quicker than the most current state-of-the-art techniques like Shan's. ADRA [46] and Liang et al. [65]. Oskar son et al., [63], Shibata et al. The processing duration for our approach is also similar to that of Durand et al.'s [20] approach. Keep in mind that a highly refined algorithm of bidirectional filtration is largely responsible for the rapid calculation of the Durand et al. First, we designate the image's geographic area as N, and the luminosity level as K, so that we can compare the time requirements of the various approaches. Fast bidirectional filtering is the foundation of the techniques of Durand et al. [20] and Kuang et al. [23], both of which can be executed in O (KNlog (KN)) time.

To further accelerate the bidirectional filtration, Durand et al. subsample the picture. For a picture, Oskar son's [69] technique requires O (K2 1K2) time, where K1 is the input luminance and K2 is the output luminance. As the number of picture pixels N is much larger than K1 and K2, Oskar son's technique typically requires less computational time. However, the technique of Shan et al. requires more processing due to handling bigger linear systems, while the method of Liang et al. has a middling numerical complexity, with the most difficult portion costing O(Nlog(N)). Finally, like Liang et al. [65], the proposed method has an O(Nlog(N)) time complexity for TV-based picture segmentation. However, the suggested method is faster in the other parts of the algorithm.

INTERNATIONAL JOURNAL OF APPLIED SCIENCE ENGINEERING AND MANAGEMENT

ISSN 2454-9940

www.ijasem.org

Vol 18, Issue 3, 2024

https://zenodo.org/records/14506032

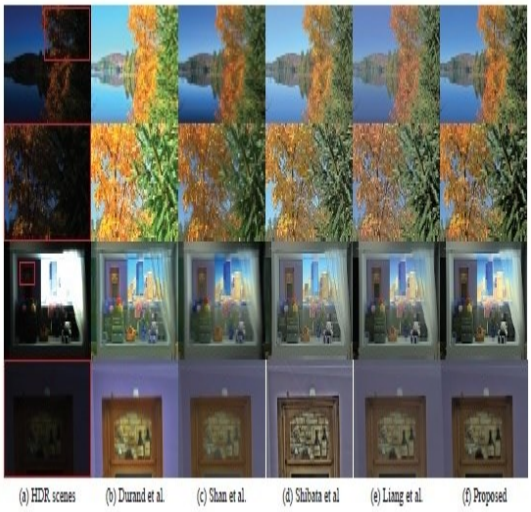

Figure 14: Additional similarities to modern HDR tone mapping techniques, such as those of Durand et al. [20], Shan et al. [63], Shibata et al. [64], and Liang et al. [65]. The HDR pictures used as input are proportionally resized to better display the details of the landscape.

II. TABLE

The HDRPS dataset consists of 105 HDR images, and the computational time required to process each image was compared using MATLAB codes. HERE WE USE A COMPUTER WITH AN INTEL CORE I7 PROCESSOR, 4.0 GHZ, AND 16 GB OF MEMORY.

Methods	Durand	Kuang	Shan	Oskarsson	Shibata	Liang	Proposed
Times (s)	**2.68**	27.93	185.90	3.6505	383.71	50.96	7.79

IV. CONCLUSION AND DISCUSSION

In this article, we suggested a paradigm for improving images that takes its cues from the sensory processes found in living organisms. In particular, the two-pathway procedure can effectively unwrap issues associated with low-quality pictures into a number of discrete jobs, such as boosting brightness, boosting details, reducing noise, etc. We also used a systematic global-to-local approach to adjust lighting, boost brightness, and calculate noise. Extensive experiments on various datasets demonstrate that the proposed method provides quite comparable performance to the recent state-of-the-art methods, but in a quite faster way, and can be used directly for nighttime and low-light image enhancement and simply extended for HDR image tone mapping. Keep in mind that the suggested approach is a picture improvement technique for low-visibility environments, so it works best on gloomy or low-light areas.

The visual naturalness of the processed pictures may suffer slightly if the black areas are brightened at the expense of the overall dynamic range of the scene. Thus, in one of our upcoming works, we plan to implement some more versatile visual adaptation methods in an effort to further boost the improved pictures' accessibility of features and visual naturalness.

REFERENCES

[1] F. Rieke and M. E. Rudd, "The challenges natural images pose for visual adaptation," Neuron, vol. 64, no. 5, pp. 605–616, 2009.

[2] Y. LeCun, Y. Bengio, and G. Hinton, "Deep learning," nature, vol. 521, no. 7553, p. 436, 2015.

[3] H. Kuang, X. Zhang, Y.-J. Li, L. L. H. Chan, and H. Yan, "Nighttime vehicle detection based on bio-inspired image enhancement and weighted score-level feature fusion," IEEE Trans. Intelligent Transportation Systems,
vol. 18, no. 4, pp. 927–936, 2017.

[4] S. M. Pizer, E. P. Amburn, J. D. Austin, R. Cromartie, A. Geselowitz, T. Greer, B. ter Haar Romeny, J. B. Zimmerman, and K. Zuiderveld, "Adaptive histogram equalization and its variations," Computer Vision, Graphics, and Image Processing, vol. 39, no. 3, pp. 355–368, 1987.

[5] Y.-T. Kim, "Contrast enhancement using brightness preserving bihistogram equalization," IEEE Trans. Consumer Electronics, vol. 43, no. 1, pp. 1–8, 1997.

[6] E. D. Pisano, S. Zong, B. M. Hemminger, M. DeLuca, R. E. Johnston, K. Muller, M. P. Braeuning, and S. M. Pizer, "Contrast limited adaptive histogram equalization image processing to improve the detection of simulated spiculations in dense mammograms," Journal of Digital Imaging, vol. 11, no. 4, pp. 193–200, 1998.

[7] T. Celik and T. Tjahjadi, "Contextual and variational contrast enhancement," IEEE Trans. Image Processing, vol. 20, no. 12, pp. 3431–3441, 2011.

[8] C. Lee, C. Lee, and C.-S. Kim, "Contrast enhancement based on layered difference representation of 2D histograms," IEEE Trans.

https://zenodo.org/records/14506032

Image Processing, vol. 22, no. 12, pp. 5372–5384, 2013.

[9] E. H. Land and J. J. McCann, "Lightness and retinex theory," Journal of the Optical Society of America A: Optics, Image Science & Vision, vol. 61, no. 1, pp. 1–11, 1971.

[10] D. J. Jobson, Z.-u. Rahman, and G. A. Woodell, "Properties and performance of a center/surround retinex," IEEE Trans. Image Processing, vol. 6, no. 3, pp. 451–462, 1997.